Head-direction coding in the hippocampal formation of birds

Elhanan Ben-Yishay[1*], Ksenia Krivoruchko[1*], Shaked Ron[1], Nachum Ulanovsky[2], Dori Derdikman[1], and Yoram Gutfreund[1,✉]

[*]These authors contributed equally to this work
[1]Department of Neurobiology, Rappaport Research Institute and Faculty of Medicine, Technion, Haifa, Israel
[2]Department of Neurobiology, Weizmann Institute of Science, Rehovot, Israel

Birds strongly rely on spatial memory and navigation. However, it is unknown how space is represented in the avian brain. Here we used tetrodes to record neurons from the hippocampal formation (*HPF*) of Japanese quails – a migratory ground-dwelling species – while the quails roamed a 1x1-meter arena (>2,100 neurons from 21 birds). Whereas spatially-modulated cells (place-cells, border-cells, etc.) were generally not encountered, the firing-rate of 12% of the neurons was unimodally and significantly modulated by the head-azimuth – i.e. these were head-direction cells (HD cells, *n=260*). Typically, HD cells were maximally active at one preferred-direction and minimally at the opposite null-direction, with preferred-directions spanning all 360°. The HD tuning was relatively broad (*mean= 130°*), independent of the animal's position and speed, and was stable during the recording-session. These findings support the existence of an allocentric head-direction representation in the quail HPF, and provide the first demonstration of head-direction cells in birds.

Correspondence: ***yoramg@technion.ac.il***

Introduction

Since the seminal discovery of place cells in the rat hippocampus (1, 2), research on the mammalian hippocampal formation has been one of the most active fields in neuroscience. Half a century of extensive research resulted in a detailed characterization of hippocampal space processing in rodents, and advanced the development of new techniques and paradigms for neural recording in behaving animals, as well as new theories and ideas on the functional role of the hippocampus (3). In addition to place cells, a whole range of other spatial cell types have been discovered in mammals, including head-direction cells (4) , spatial-view cells (5), grid cells (6, 7), border cells (8, 9), speed cells (10), and recently goal-direction cells (11). The study of spatial processing in the hippocampus was not limited to rats but expanded to other mammals, including mice, bats, monkeys and humans (12–15). The emerging notion is that the hippocampus and its related structures support spatial cognition and memory (16–18).

One important and relatively understudied question is whether the role of the hippocampal formation in spatial cognition is unique to mammals, or can we find its origins in other vertebrates? In this aspect, birds provide an interesting case study. Spatial navigation and foraging behaviors are common in avian species, and in some cases outperform those of mammals. Migratory and homing behaviors are stunning examples of bird navigational capabilities (19–23). In addition, the extraordinary food caching and retrieval behaviors found in some song birds and corvids demonstrate the impressive spatial-memory capacities of birds (24–26). What might be the neural mechanisms that support such elaborate spatial cognition in birds? And how similar are they to the hippocampal space-processing system in mammals? Answers to these questions will constitute a breakthrough in our understanding of the evolutionary origin of space processing and, through comparative studies, may contribute to understanding the underlying mechanisms and to establishing general principles of navigation and spatial memory across vertebrates.

The avian hippocampal formation (HPF), a structure in the medial dorsal cortex of the avian brain (Figure (27–31). Growing evidence suggest that it plays a role in spatial tasks (20, 22, 26, 27). For example, experiments in HPF-lesioned pigeons consistently showed deficiencies in homing behaviors (32). Similarly, lesion studies in zebra finches demonstrated that the HPF in these songbirds is involved in both learning and retention of spatial tasks (33). Investigations on the patterns of activation of immediate early genes showed enhanced activation of the HPF during retrieval of cached food items (34) – a highly demanding spatial behavior–and during maze tasks (35). Another striking indication for the involvement of avian HPF in spatial memory is found in the correlation between HPF volume and the importance of food caching for the natural behavior of the species (36). Finally, neurons with broad and multiple place-fields were reported in the pigeon hippocampal formation, although these fields were mostly associated with rewarded locations (37–39). These raise the hypothesis that the role of the mammalian hippocampus in spatial cognition and the underlying neural spatial representation (place cells, grid cells, etc.) have their roots in earlier vertebrate evolution. However, a clear allocentric representation of space has not yet been found in either the avian hippocampus, or any other non-mammalian vertebrate. In this study we report results of single unit recordings in the hippocampal formation of Japanese quails (Coturnix japonica), showing clear (yet broad) head-directional tuning signals. The Japanese quail is a ground-dwelling foraging bird, which has been extensively used as an animal model in developmental biology (41). However, to our knowledge, single unit recordings in behaving quails have not been done before. We used tetrode microdrives to perform electrophysiological recordings in freely-behaving

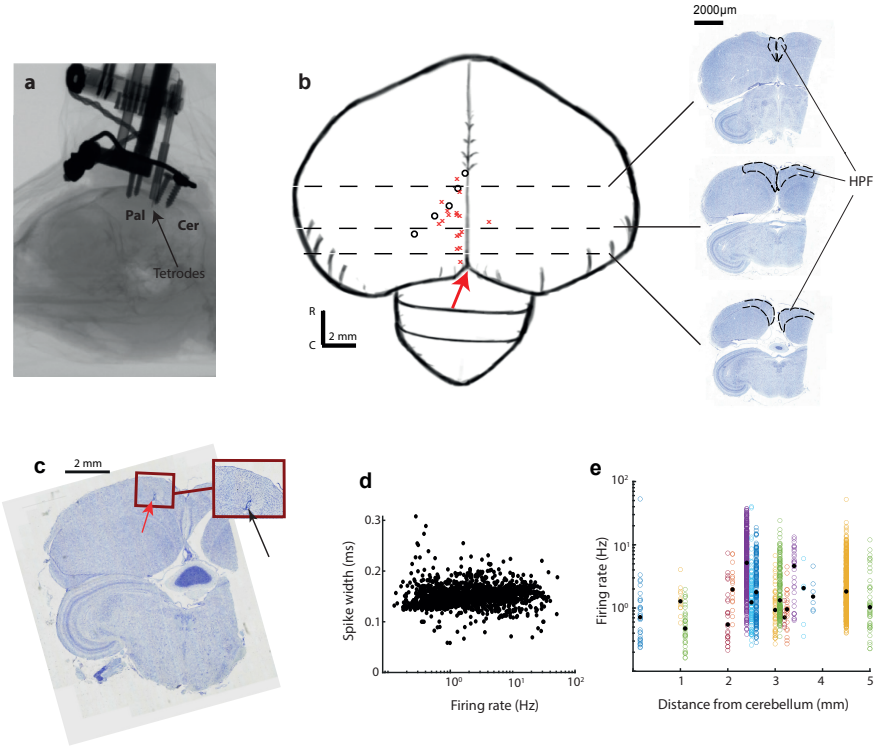

Fig. 1. Recording locations and firing properties. a, Micro-CT scan showing an implanted microdrive on the quail's skull. Arrow points to the tip of the tetrodes. *Pal*-pallium, *Cer*-cerebellum. **b**, A sketch of the quail's brain. Red X's mark the approximate recording locations from 17 quails. Black dots represent the putative lateral border of the HPF, which follows the lateral end of the lateral ventricle. Distances of black circles from the midline are based on the quail's brain stereotaxic atlas (40). Dashed lines indicate the approximate coronal section levels shown on the right. The dashed lines in the insets mark the HPF region. **c**, A Nissl stained coronal section showing an electrolytic lesion. The red arrow points to the lateral tip of the lateral ventricle. Inset: magnified view of the lesioned region. **d**, Spike width (full width at half maximum) for all the recorded single-units as a function of their firing rate. X-axis is logarithmic. **e**, Firing rates of single-units versus the recording location along the rostro-caudal axis (rostral distance from cerebellum tip). Colors designate different quails. Black circles designate the median firing rates. Y-axis is logarithmic.

quails that explored a square arena, while we tracked their position and head-direction. Analysis of more than 2000 putative single-units in the HPF revealed that about 12% of the recorded cells showed a statistically significant head-direction response, which maintained stability over time, space, and across speeds. However, we were not able to detect significant spatially-modulated cells (e.g. place cells). We thus provide the first evidence for a head-direction system in an avian species, shedding new light on the evolutionary and functional homology of the hippocampal system across taxa. across taxa.

Results

No evidence for rodent-like place cells in the hippocampal formation of quails. We recorded and isolated 2132 single units from 21 quails. In several of the quails, the signal-to-noise levels of the units were substantially reduced in the days following the surgery – hence the large variation in the number of cells collected from each quail – from 4 cells in quail 30 to 514 cells in quail 24 (Supplementary Table S1). Tetrodes were implanted in the left hemisphere in 20 out of the 21 quails and were stereotactically targeted to a zone within 5 mm rostrally from the cerebellar rostral tip, and within 2 mm laterally to the midline (Fig. 1a-b). 17 Penetration locations were reconstructed post-mortem by measuring the rostral and lateral distances of the penetration sites from the rostral tip of the cerebellum (Fig. 1b). In four of the quails we do not have a post-mortem measurement of the penetration site. In 4 quails the tetrode track was reconstructed with an electrolytic lesion (Fig. 1c). Across the recorded population, firing rates and spike widths varied; but we could not detect systematic clustering of cell spike types (Fig. 1d) nor systematic variation of firing-rates along the rostro-caudal axis (Fig. 1e).

During the experiments, the quails sometimes explored the arena relatively evenly and sometimes in a restricted manner (Fig. 2a and Supplementary Fig. S1). In many cases, such as the example cell shown in Figure 2, the firing rate as a function of the quail's position (rate map) displayed broad spatial firing across the arena (Fig. 2b). In this example cell, spatial information was not statistically significant (spatial information was smaller than the 99th percentile of the shuffles). Only 19 cells (out of 938 cells that were recorded in behavioral sessions where the quail covered more than 50% of the arena) passed the criteria for place cells (spatial information larger than the 99th percentile of the shuffles [p<0.01]). These

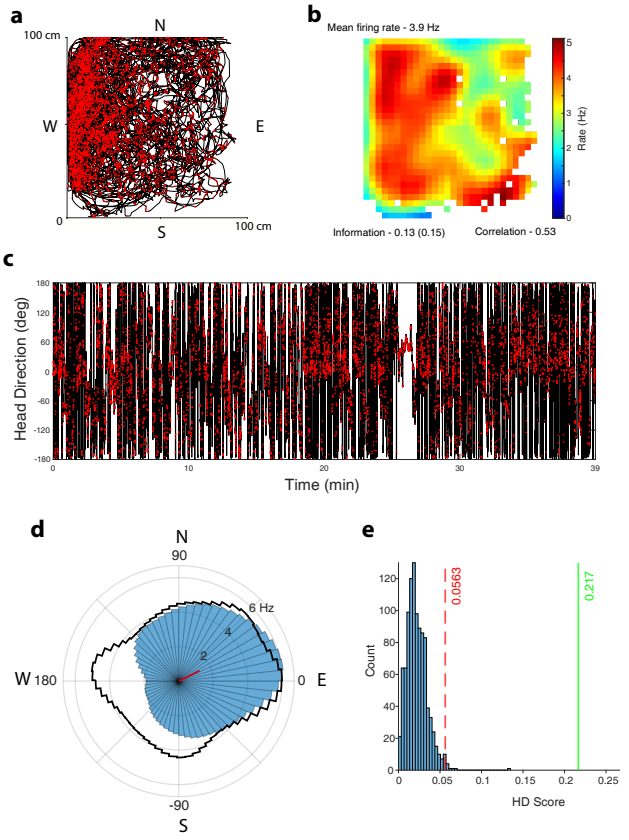

Fig. 2. Data from an example neuron. a, The quail's position in the arena during a 35-min recording session is marked by a black line. Red dots are the locations of spikes fired by the neuron. N-north side of the arena; S-south, E-east; W-west. **b**, Rate map of the neuron. Indicated are the mean firing rate (top left), spatial information (bottom left), and map correlation between first and second half of the session (bottom right). White pixels are pixels which were not visited at least 200 msec during the session. **c**, Head-direction of the quail as a function of time (black line), with spikes superimposed (red dots). **d**, Polar plot showing the firing rate as a function of head direction. The red bar indicates the length and direction of the Rayleigh vector. The black curve shows the relative time spent in each head-direction bin. **e**, Rayleigh score (HD score) shuffling histogram. Red dashed line represents the HD score for the 99% percentile shuffle; green line shows the observed HD score for this example neuron.

neurons mostly did not display a clear single field of activity in their rate-maps (Supplementary Fig. S2). Therefore, we did not pursue further analysis of place modulations in this study.

Head-direction cells in the hippocampal formation of quails. We next moved to analyzing the relationship between the firing rate and the head direction. In the example cell, firing rate was clearly modulated by the head direction (Fig. 2c), rising from 2 Hz Hz at 180° azimuth to more than 6 Hz Hz at 10° azimuth (Fig. 2d). The Rayleigh vector length (see Methods; termed thereafter 'HD score') of the cell was 0.217; when compared to 1000 shuffled spike-trains, the observed HD score was well above the 99th percentile of the shuffled distribution (Fig. 2e) – and thus we categorized this example cell as having a significant HD response ($p<0.01$). The best direction of the cell (computed as the direction of the Rayleigh vector) pointed roughly North-East (red bar in Fig.3 2d).

Out of the total recorded population, 260 cells (12%) passed the shuffling statistical test as head direction cells (with a chance level of 1%; Supplementary Table S1). To confirm that the number of HD cells is not biased by the parameters used to define a single-unit (isolation distance and L-ratio criteria; see Methods), we analyzed the percentage of HD cells at 8 different combinations of criteria (Supplementary Table S2). The value of roughly 12% HD cells was maintained regardless of the combination of criteria used.

Stability and distribution of best directions. In general, the HD modulation tended to be relatively broad (Fig. 3a). The mean tuning-width (width at half height, measured halfway between maximum and minimum of the tuning) for the population of significant HD cells was 130.4 ± 54 (Fig. 3b). Moreover, the modulation depth (normalized difference between the highest and lowest firing rate) varied between 0.4 and 1, with a mean of 0.66 (Fig. 3c). Importantly, the HD tuning curves showed high stability: (i) The best directions in the first and second halves of the session were significantly correlated (Fig. 3d; Pearson correlation test: r=0.95, p<0.0001, n=186; the numbers of neurons in this and following comparisons is lower than n=260 because we required sufficient coverage in both halves: Methods). (ii) The best directions from the north and south halves as well as the west and east halves of the arena were significantly correlated (Fig. 3e and 3f, respectively; Pearson correlation test, r=0.88, p<0.0001, n=175; and r=0.90, p<0.0001, n=169). (iii) Because some of the quails mostly explored the borders of the arena (see examples in Supplementary Fig. S1), we also analyzed the best head directions when the quails were near the border versus when they were in the center of the arena; these were also found to be highly significantly correlated (Fig. 3g; Pearson correlation test: r=0.88, p<0.0001, n=122). (iv) Finally, the best directions during fast movement of the quail (>10 cm/sec) were significantly correlated with best directions during slow movements (<10 cm/sec) (Fig. 3h; Pearson correlation test: r=0.98, p<0.0001, n=201). In all these tests the regression line was very close to the 45° line (Fig. 3d-h: compare red and black lines). Our results indicate a stable head-direction representation over time and space, as well as over the speed of the quails. The significant correlation between the best directions in different parts of the arena argue against the possibility that the head-direction tuning is an outcome of spatial view cells (42). This conclusion was further corroborated by a simulation of spatial view cells in the arena (Supplementary Fig. S3).

The best directions covered almost uniformly the entire range of 360° (Fig. 4a). This uniformity was seen when pooling data from all quails (Fig. 4a), as well as in most of the individual quails (Supplementary Fig. S5). Significant HD cells, spanning all possible directions, have been recorded at all the recording-depths in the HPF and at all anatomical locations within HPF (Figs 4b-c). HD cells were found at nearly all depths from surface and all distances rostral to the cerebellum tip (Figs. 4d-e). Thus, our results do not indicate a clear

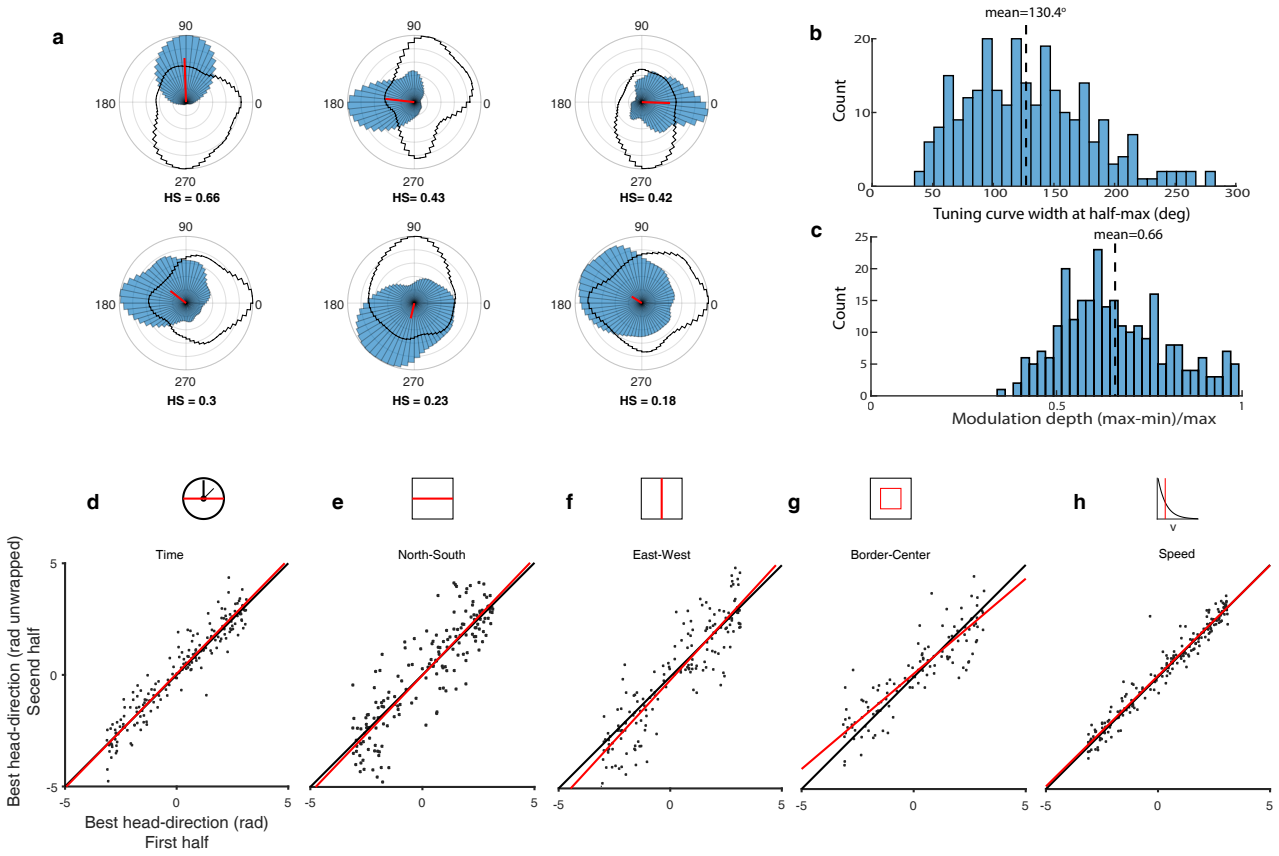

Fig. 3. Head-direction cells characteristics and stability. **a**, Examples of six cells significantly modulated by head-direction, organized in descending order by their HD score (HS; its value is indicated below each neuron). Blue histograms represent the polar firing-rate curve. Black line depicts the time spent in each direction (behavioral curve). Curves are normalized to their maximum. **b**, Distribution of the tuning curve widths (width at half maximum) of the head direction firing-rate curves. The dashed line represents the mean. **c**, Distribution of the modulation depths (maximal firing-rate minus the minimal firing rate, normalized by the maximal firing rate). The dashed line represents the mean. **d-h**, Population scatter plots for HD cells, comparing the best head-directions (direction of Rayleigh vector) in the first half versus the second half of the session **(d)**, The north versus south parts of the arena **(e)**, east versus west parts of the arena **(f)**, near border versus center of the arena **(g)** and finally, fast speeds versus slow speeds **(h)**. Black lines are the identity-lines (equal directions) and red lines show the linear regressions.

tendency for anatomical clustering of HD cells or anatomical clustering of best directions. We conclude that significant and stable HD cells are found throughout the HPF of quails.

Discussion

To our knowledge, this is the first time that a stable and abundant population of head-direction cells is reported in the hippocampal formation of an avian species. Neurons that represent head direction in allocentric coordinates during real-world movements have been reported in mammals (4, 43–45), and very recently in fish (46) – as well as in head-fixed insects in virtual reality (47, 48). These cells are thought to underlie the directional sense of animals, which is vitally important for goal directed navigation and other spatially coordinated behaviors (49). Because many species of birds display remarkable cognitive capabilities that are related to spatial behaviors and spatial memory (19–23, 25), an elaborated head direction system is expected in avian brains. However, up until now such a system has not been discovered. A characteristic of systems representing head direction is that they exhibit a uniform and stable representation of directions (49, 50). Moreover, direction sensitivity is maintained independent of the speed of the animal (4). Here we report a population of neurons that are modulated by the head direction of the quail in allocentric space: these neurons uniformly represent all directions, and their preferred direction is stable across time, space, and movement speeds. We therefore posit that these cells are part of a head-direction system in quails, perhaps homologous to that of mammals.

Networks of head-direction cells in mammals integrate angular velocity information coming from the vestibular system with environmental cues from the visual system (51). This integration is believed to take place in the dorsal presubiculum (52), anterodorsal thalamus, and lateral mammillary nucleus (53). The head-direction information is conveyed from the dorsal presubiculum to the entorhinal cortex, where it interacts with other spatial information coming from the hippocampus (54, 55). The detailed circuit of the avian HPF, unlike its homologous mammalian structure, is not well characterized (27). Atoji and Wild ((29, 56)) provided a histochemical division of the pigeon HPF to dorsal lateral (DL), dorsal medial (DM) and a medial V shape complex. The homology of this subdivision with the mammalian HPF is debated, with the controversy focused mostly around the homologies of the V-shaped complex and the dorsal medial parts with the mammalian Dentate Gyrus and Ammon's horn (57–61). How-

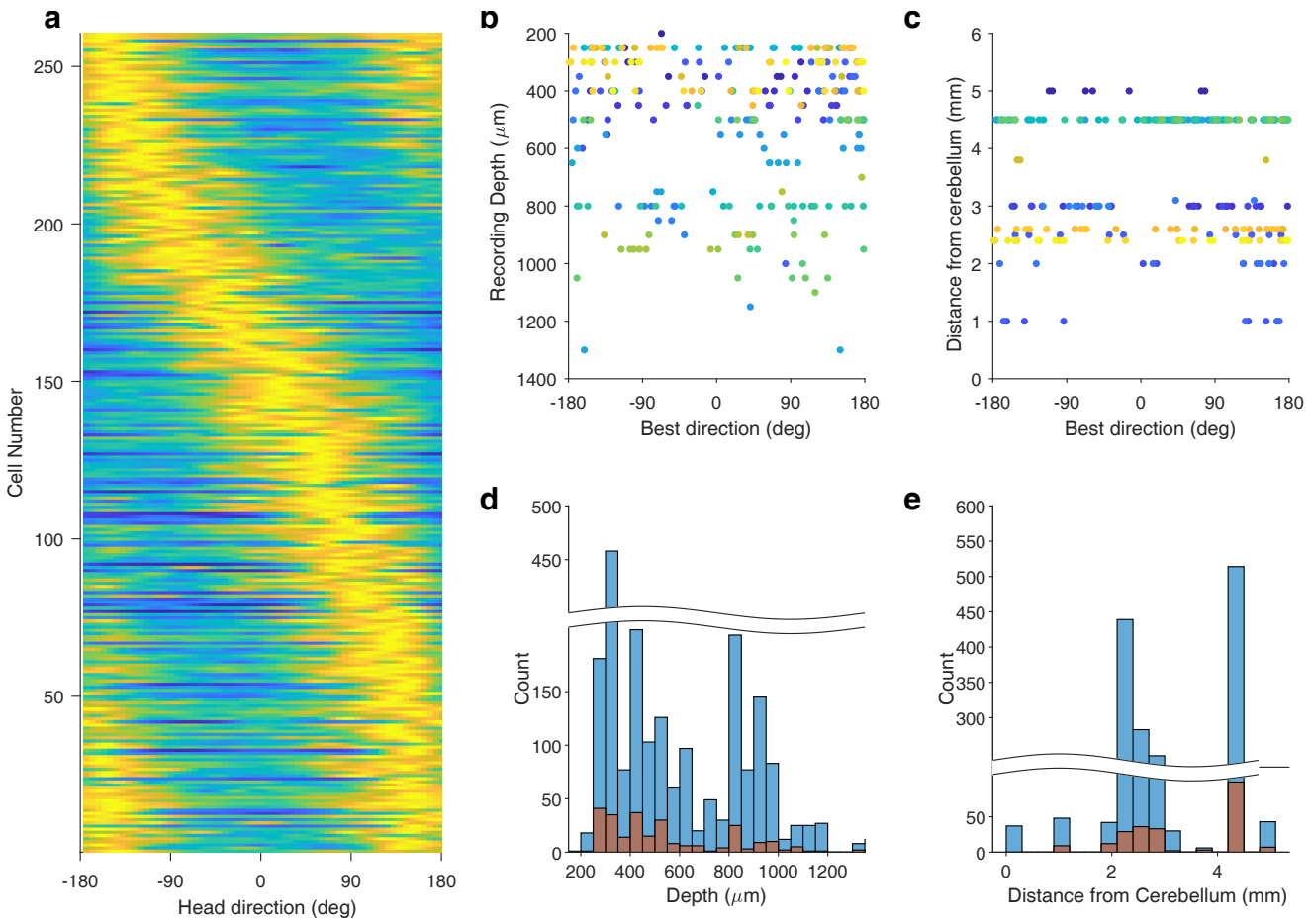

Fig. 4. Distributions of best directions in the population of head-direction cells. a, Normalized HD tuning-curves for all significant head-direction cells (n=260). Curves are ordered according to the best direction. **b**, Best directions of HD cells as a function of estimated recording depth. Colors designate different quails. **c**, Best directions as a function of recording distance from the cerebellum along the rostro-caudal axis. Colors indicate different quails. **d**, Histograms of total number of single units recorded (blue) and number of HD cells (orange) as a function of recording depth. **e**, Same as **d** but as a function of recording distance from the cerebellum.

ever, there seems to be an agreement regarding the DL being related to the mammalian subiculum and entorhinal cortex (27, 29, 62–64). Many of the HD cells that we recorded were in the more accessible dorsal lateral (DL) and dorsal medial (DM) parts of the HPF (Fig. 1b and Fig. 4b) – thus, our findings possibly represent an avian head-direction system homologous to the subiculum/entorhinal HD system of mammals. Notably, the DL and DM portions of the HPF receive connections from visual Wulst (65) as well as connections from the dorsal thalamus (66), which may provide the anatomical substrates for integration of visual and self-motion cues. Yet, obvious differences exist between our findings and analogous reports in rodents: (1) Most notably, many of the HD cells in the entorhinal cortex and subiculum of mammals fire close to zero spikes (< 0.5 Hz) in the null directions (67, 68), whereas in our population of HD cells the neurons had a non-zero baseline firing at all head directions, with significantly higher rates in the preferred direction as compared to the null directions. (2) Moreover, in the subiculum and medial entorhinal cortex of rodents many of the neurons are narrowly tuned (<45°at half peak) (67). Such narrowly tuned neurons were a small fraction of our population of HD cells – while most of the quail's HD cells were more broadly tuned. (3) In addition to the above-mentioned differences, the abundance of HD cells in the avian HPF was lower than in the mammalian subiculum and layers III to VI of medial entorhinal cortex, where more than 40% of the neurons are significant HD cells (68, 69) – compared to about 12% of the recorded cells in the quail. The relatively low abundance of HD cells may reflect the non-focal sampling of neurons in our study: Perhaps a higher fraction of HD cells would be found in specific sub regions of the HPF. However, our results showed no evidence for anatomical clustering of HD cells in the quail's HPF (Fig. 4d-e).

Another striking difference between neural responses in rodents and the results reported here is the apparent lack of clear place, grid and border cells. Few neurons showed spatial modulation of their firing rates, but these were mostly broadly tuned. These results are consistent with results from Bingman and colleagues (37–39), which studied the HPF of pigeons in radial mazes and open arenas. The results of these previous studies showed scarce spatial modulation, consistent with multiple broad fields, which were related mostly to rewarded locations. A recent electrophysiological survey of Zebra Finch HPF also failed to identify place cells (70). On the other hand, behavioral experiments in quails (71),

pigeons (72) and zebra finches (73) strongly support well-developed spatial cognitive abilities in these bird species – such as novel shortcuts, model-based spatial learning, navigation and spatial memory. It is possible that the spatial perception of birds is not located in the HPF, or alternatively, in a specific sub region of the HPF which has not been explored yet. However, lesion studies in quails, pigeons and zebra finches (33, 74, 75), as well as gene expression analysis (76, 77), provide strong evidence that the HPF of birds is critically important for spatial cognition. A different possibility is that the HPF of mammals and birds holds the neural basis of spatial cognition, but evolved differently: rather than having a large population of highly-specific and sparsely encoding cells – as seen in mammals – birds might possess a population-coding scheme which is carried by a population of neurons with broad tuning and non-uniform fields. This possibility is consistent with our findings of head direction tuning which was broadly tuned. A recent study in food caching birds that are specialized in spatial memory (chickadees and tufted titmouses) revealed place cells in the rostral HPF (70), in the same areas that have been explored in other birds, including here in quails – but without observing place cells. Taken together, our and previous findings suggest the notion that the HPF in birds generally supports spatial cognition – but that the detailed coding scheme is species-specific and evolved differently according to the ecological needs of the species. One possibility is that quails, which are migratory birds in origin (78) – and which need to maintain constant directional bearing during migration – have evolved a more developed HD-cell representation as compared to other, non-migratory, bird species. These interesting inter-species differences call for further comparative investigations of spatial cell types across vertebrates, and linking it to the animals' behavioral repertoire and evolutionary history: A merging of neuroscience, evolution, and behavioral ecology.

ACKNOWLEDGEMENTS

We thank Dr. Yael Zahar for assistance and support. This work was supported by research grants from the Rappaport Institute for Biomedical Research, the Adelis Foundation and the Israel Science Foundation. Yoram Gutfreund also acknowledges the generous support of the Edward S. Mueller Eye Research Fund.

Bibliography

1. J. O'Keefe and J. Dostrovsky. The hippocampus as a spatial map. Preliminary evidence from unit activity in the freely-moving rat. *Brain Res*, 34:171–175„ 1971. doi: doi:0006-8993(71)90358-1.
2. J. O'Keefe and L. Nadel. *The hippocampus as a cognitive map*. Clarendon Press; Oxford University Press, 1978.
3. H. Eichenbaum. The role of the hippocampus in navigation is memory. *J Neurophysiol*, 117: 1785–1796„ 2017. doi: 10.1152/jn.00005.2017.
4. J. S. Taube, R. U. Muller, and J. B. Ranck. Head-direction cells recorded from the postsubiculum in freely moving rats. I. Description and quantitative analysis. *Journal of Neuroscience*, 10(2):420–435, February 1990. ISSN 0270-6474, 1529-2401. doi: 10.1523/JNEUROSCI.10-02-00420.1990. Publisher: Society for Neuroscience Section: Articles.
5. E.T. Rolls, R.G. Robertson, and P. GeorgesFrancois. Spatial view cells in the primate hippocampus. *European Journal of Neuroscience*, 9:1789–1794, 1997.
6. M. Fyhn, S. Molden, M.P. Witter, E.I. Moser, and M.B. Moser. Spatial representation in the entorhinal cortex. *Science*, 305:1258–1264, 2004.
7. T. Hafting, M. Fyhn, S. Molden, M.B. Moser, and E.I. Moser. Microstructure of a spatial map in the entorhinal cortex. *Nature*, 436:801–806, 2005.
8. T. Solstad, C. Boccara, E. Kropff, M.B. Moser, and E.I. Moser. Representation of Geometric Borders in the Entorhinal Cortex. *Science*, 322:1865–1868, 2008.
9. C. Lever, S. Burton, A. Jeewajee, J. O'Keefe, and N. Burgess. Boundary Vector Cells in the Subiculum of the Hippocampal Formation. *J. Neurosci*, 29:9771–9777„ 2009. doi: 10.1523/jneurosci.1319-09.2009.
10. E. Kropff, J.E. Carmichael, M.B. Moser, and E.I. Moser. Speed cells in the medial entorhinal cortex. *Nature*, 523:419–424„ 2015. doi: 10.1038/nature14622.
11. A. Sarel, A. Finkelstein, L. Las, and N. Ulanovsky. Vectorial representation of spatial goals in the hippocampus of bats. *Science*, 355:176–180, 2017.
12. M. Fyhn, T. Hafting, M.P. Witter, E.I. Moser, and M.-B. Moser. Grid cells in mice. *Hippocampus*, 18:1230–1238, 2008.
13. J. Jacobs. Direct recordings of grid-like neuronal activity in human spatial navigation. *Nature Neuroscience*, 16:1188–1190, 2013.
14. M.M. Yartsev, M.P. Witter, and N. Ulanovsky. Grid cells without theta oscillations in the entorhinal cortex of bats. *Nature*, 479:103–107, 2011.
15. N.J. Killian, M.J. Jutras, and E.A. Buffalo. A map of visual space in the primate entorhinal cortex. *Nature*, 491:761–764, 2012.
16. D. Derdikman and J.J.Space Knierim. *Time and Memory in the Hippocampal Formation*. Springer, 2014.
17. M.I. Anderson. Behavioral correlates of the distributed coding of spatial context. *Hippocampus*, 16:730–742„ 2006. doi: 10.1002/hipo.20206.
18. M. Geva-Sagiv, L. Las, Y. Yovel, and N. Ulanovsky. Spatial cognition in bats and rats: from sensory acquisition to multiscale maps and navigation. *Nat Rev Neurosci*, 16:94–108„ 2015. doi: 10.1038/nrn3888.
19. W. Wiltschko and R. Wiltschko. Global navigation in migratory birds: tracks, strategies, and interactions between mechanisms. *Curr Opin Neurobiol*, 22:328–335„ 2012. doi: 10.1016/j.conb.2011.12.012.
20. H. Mouritsen, D. Heyers, and O. Gunturkun. The Neural Basis of Long-Distance Navigation in Birds. *Annu Rev Physiol*, 2015. doi: 10.1146/annurev-physiol-021115-105054.
21. K. Thorup. Evidence for a navigational map stretching across the continental US in a migratory songbird. *Proceedings of the National Academy of Sciences*, 104:18115–18119, 2007.
22. H.G. Wallraff and H.G. Wallraff. *Avian navigation: pigeon homing as a paradigm*. Springer Science & Business Media, 2005.
23. Verner P. Bingman, Gerald E. Hough, Meghan C. Kahn, and Jennifer J. Siegel. The homing pigeon hippocampus and space: in search of adaptive specialization. *Brain, Behavior and Evolution*, 62(2):117–127, 2003. ISSN 0006-8977. doi: 10.1159/000072442.
24. U. Grodzinski and N.S. Clayton. Problems faced by food-caching corvids and the evolution of cognitive solutions. *Philosophical Transactions of the Royal Society B: Biological Sciences*, 365:977–987, 2010.
25. S.D. Healy and T.A. Hurly. Spatial learning and memory in birds. *Brain Behav Evol*, 63: 211–220„ 2004. doi: 10.1159/000076782.
26. S.D. Healy, S.R. Kort, and N.S. Clayton. The hippocampus, spatial memory and food hoarding: a puzzle revisited. *Trends in ecology & evolution*, 20:17–22, 2005.
27. C. Herold, V.J. Coppola, and V.P. Bingman. The maturation of research into the avian hippocampal formation: Recent discoveries from one of the nature's foremost navigators. *Hippocampus*, 25:1193–1211„ 2015. doi: 10.1002/hipo.22463.
28. H.J. Karten. Organization of Avian Telencephalon and Some Speculations on Phylogeny of Amniote Telencephalon. *Annals of the New York Academy of Sciences*, 167:164–167, 1969.
29. Y. Atoji and J.M. Wild. Anatomy of the avian hippocampal formation. *Rev Neurosci*, 17: 3–15, 2006.
30. C.C. Chen, C.M. Winkler, A.R. Pfenning, and E.D. Jarvis. Molecular profiling of the developing avian telencephalon: regional timing and brain subdivision continuities. *J Comp Neurol*, 521:3666–3701„ 2013. doi: 10.1002/cne.23406.
31. M. Colombo and N. Broadbent. Is the avian hippocampus a functional homologue of the mammalian hippocampus? *Neurosci Biobehav Rev*, 24:465–484, 2000.
32. A. Gagliardo, P. Ioale, and V.P. Bingman. Homing in pigeons: the role of the hippocampal formation in the representation of landmarks used for navigation. *J Neurosci*, 19:311–315, 1999.
33. S. Watanabe and H.J. Bischof. Effects of hippocampal lesions on acquisition and retention of spatial learning in zebra finches. *Behav Brain Res*, 155:147–152„ 2004. doi: 10.1016/j.bbr.2004.04.007.
34. T.V. Smulders and T.J. DeVoogd. Expression of immediate early genes in the hippocampal formation of the black-capped chickadee (Poecile atricapillus) during a food-hoarding task. *Behav Brain Res*, 114:39–49, 2000.
35. U. Mayer and H.J. Bischof. Brain activation pattern depends on the strategy chosen by zebra finches to solve an orientation task. *J Exp Biol*, 215:426–434„ 2012. doi: 10.1242/jeb.063941.
36. V.V. Pravosudov and T.V. Smulders. Integrating ecology, psychology and neurobiology within a food-hoarding paradigm. *Philos Trans R Soc Lond B Biol Sci*, 365:859–867„ 2010. doi: 10.1098/rstb.2009.0216.
37. G.E. Hough and V.P. Bingman. Spatial response properties of homing pigeon hippocampal neurons: correlations with goal locations, movement between goals, and environmental context in a radial-arm arena. *J Comp Physiol A Neuroethol Sens Neural Behav Physiol*, 190:1047–1062„ 2004. doi: 10.1007/s00359-004-0562-z.
38. M.C. Kahn, J.J. Siegel, T.J. Jechura, and V.P. Bingman. Response properties of avian hippocampal formation cells in an environment with unstable goal locations. *Behav Brain Res*, 191:153–163„ 2008. doi: 10.1016/j.bbr.2008.03.023.
39. J.J. Siegel, D. Nitz, and V.P. Bingman. Lateralized functional components of spatial cognition in the avian hippocampal formation: evidence from single-unit recordings in freely moving homing pigeons. *Hippocampus*, 16:125–140„ 2006. doi: 10.1002/hipo.20139.
40. J. Baylé. Stereotaxic topography of the brain of the quail. *J Physiol Paris*, 68:219–241, 1974.
41. G. Poynter, D. Huss, and R. Lansford. *Japanese quail: an efficient animal model for the production of transgenic avians*. Cold Spring Harbor Protocols, 2009.
42. E.T. Rolls. Spatial view cells and the representation of place in the primate hippocampus. *Hippocampus*, 9:467–480, 1999.
43. A. Finkelstein. Three-dimensional head-direction coding in the bat brain. *Nature*, 517:159–164, 2015.
44. J. S. Taube, R. U. Muller, and J. B. Ranck. Head-direction cells recorded from the post-

subiculum in freely moving rats. II. Effects of environmental manipulations. *The Journal of Neuroscience: The Official Journal of the Society for Neuroscience*, 10(2):436–447, February 1990. ISSN 0270-6474.

45. R. G. Robertson, E. T. Rolls, P. Georges-François, and S. Panzeri. Head direction cells in the primate pre-subiculum. *Hippocampus*, 9(3):206–219, 1999. ISSN 1050-9631. doi: 10.1002/(SICI)1098-1063(1999)9:3<206::AID-HIPO2>3.0.CO;2-H.
46. E. Vinepinsky. Representation of Borders and Swimming Kinematics in the Brain of Freely-Navigating Fish. *bioRxiv*, 291013, 2019. doi: 10.1101/291013.
47. J.D. Seelig and V. Jayaraman. Neural dynamics for landmark orientation and angular path integration. *Nature*, 521:186–191,, 2015. doi: 10.1038/nature14446.
48. D.B. Turner-Evans and V. Jayaraman. The insect central complex. *Current Biology*, 26:453–457, 2016.
49. R.G. Munn and L.M. Giocomo. Multiple head direction signals within entorhinal cortex: origin and function. *Current Opinion in Neurobiology*, 64:32–40, 2020.
50. K.E. Cullen and J.S. Taube. Our sense of direction: progress, controversies and challenges. *Nature Neuroscience*, 20:1465, 2017.
51. B.K. Hulse and V. Jayaraman. Mechanisms Underlying the Neural Computation of Head Direction. *Annual Review of Neuroscience*, 43, 2019.
52. R.M. Yoder, B.J. Clark, and J.S. Taube. Origins of landmark encoding in the brain. *Trends in Neurosciences*, 34:561–571, 2011.
53. B.J. Clark and J.S. Taube. Vestibular and attractor network basis of the head direction cell signal in subcortical circuits. *Frontiers in neural circuits*, 6, 7, 2012.
54. J.S. Taube. The head direction signal: Origins and sensory-motor integration. *Annual Review of Neuroscience*, 30:181–207,, 2007. doi: 10.1146/annurev.neuro.29.051605.112854.
55. S.S. Winter, B.J. Clark, and J.S. Taube. Disruption of the head direction cell network impairs the parahippocampal grid cell signal. *Science*, 347:870–874, 2015.
56. Y. Atoji and J.M. Wild. Fiber connections of the hippocampal formation and septum and subdivisions of the hippocampal formation in the pigeon as revealed by tract tracing and kainic acid lesions. *J Comp Neurol*, 475:426–461,, 2004. doi: 10.1002/cne.20186.
57. J.R. Krebs, J.T. Erichsen, and V.P. Bingman. The distribution of neurotransmitters and neurotransmitter-related enzymes in the dorsomedial telencephalon of the pigeon (Columba livia. *Journal of Comparative Neurology*, 314:467–477, 1991.
58. G. Kempermann. New neurons for'survival of the fittest'. *Nature reviews neuroscience*, 13: 727–736, 2012.
59. G.F. Striedter. Evolution of the hippocampus in reptiles and birds. *J Comp Neurol*, 524: 496–517,, 2016. doi: 10.1002/cne.23803.
60. C. Herold. Distribution of neurotransmitter receptors and zinc in the pigeon (Columba livia) hippocampal formation: a basis for further comparison with the mammalian hippocampus. *Journal of Comparative Neurology*, 522:2553–2575, 2014.
61. Y. Atoji, S. Sarkar, and J.M. Wild. Proposed homology of the dorsomedial subdivision and V-shaped layer of the avian hippocampus to Ammon's horn and dentate gyrus, respectively. *Hippocampus*, 26:1608–1617,, 2016. doi: 10.1002/hipo.22660.
62. A.D. Székely. The avian hippocampal formation: subdivisions and connectivity. *Behavioural brain research*, 98:219–225, 1999.
63. J.J. Siegel, D. Nitz, and V.P. Bingman. Electrophysiological profile of avian hippocampal unit activity: a basis for regional subdivisions. *Journal of Comparative Neurology*, 445:256–268, 2002.
64. N.C. Rattenborg and D. Martinez-Gonzalez. A bird-brain view of episodic memory. *Behavioural brain research*, 222:236–245, 2011.
65. M. Shanahan, V.P. Bingman, T. Shimizu, M. Wild, and O. Gunturkun. Large-scale network organization in the avian forebrain: a connectivity matrix and theoretical analysis. *Front Comput Neurosci*, 7:89,, 2013. doi: 10.3389/fncom.2013.00089.
66. C. Trottier, J. Reperant, and D. Miceli. Anatomical evidence of a retino-thalamo-hippocampal pathway in the pigeon (Columba livia. *Journal fur Hirnforschung*, 36:489–500, 1995.
67. F. Sargolini. Conjunctive representation of position, direction, and velocity in entorhinal cortex. *Science*, 312:758–762, 2006.
68. L.M. Giocomo. Topography of head direction cells in medial entorhinal cortex. *Curr Biol*, 24: 252–262,, 2014. doi: 10.1016/j.cub.2013.12.002.
69. C.N. Boccara. Grid cells in pre- and parasubiculum. *Nature Neuroscience*, 13:987–994,, 2010. doi: 10.1038/nn.2602.
70. H.L. Payne and A. D. Interaction of place and gaze representations in the hippocampus of food-caching birds. In . *Society for Neuroscience Meeting 2019*, 2019.
71. T. Ruploh, A. Kazek, and H.J. Bischof. Spatial orientation in Japanese quails (Coturnix coturnix japonica. *PLoS One*, 6, e28202, 2011. doi: 10.1371/journal.pone.0028202.
72. K. Cheng, M.L. Spetch, D.M. Kelly, and V.P. Bingman. Small-scale spatial cognition in pigeons. *Behavioural Processes*, 72:115–127, 2006.
73. U. Mayer, S. Watanabe, and H.J. Bischof. Spatial memory and the avian hippocampus: research in zebra finches. *J Physiol Paris*, 107:2–12,, 2013. doi: 10.1016/j.jphysparis.2012.05.002.
74. F. Lormant. Role of the hippocampus in spatial memory in Japanese quail. *Poultry science*, 2019.
75. V.P. Bingman and G. Yates. Hippocampal lesions impair navigational learning in experienced homing pigeons. *Behav Neurosci*, 106:229–232,, 1992. doi: 10.1037//0735-7044.106.1.229.
76. U. Mayer, S. Watanabe, and H.J. Bischof. Hippocampal activation of immediate early genes Zenk and c-Fos in zebra finches (Taeniopygia guttata) during learning and recall of a spatial memory task. *Neurobiol Learn Mem*, 93:322–329,, 2010. doi: 10.1016/j.nlm.2009.11.006.
77. D.F. Sherry, S.L. Grella, M.F. Guigueno, D.J. White, and D.F. Marrone. Are There Place Cells in the Avian Hippocampus? *Brain, behavior and evolution*, 90:73–80, 2017.
78. S. DERÉGNAUCOURT, J.-C. GUYOMARC'H, and M. BELHAMRA. Comparison of migratory tendency in European Quail Coturnix c. coturnix, domestic Japanese Quail Coturnix c. japonica and their hybrids. *Ibis*, 147:25–36,, 2005. doi: 10.1111/j.1474-919x.2004.00313.x.
79. H.J. Karten and W. Hodos. *A stereotaxic atlas of the pigeon brain*. The Johns Hopkins Press, 1967.
80. S. Weiss. Consistency of spatial representations in rat entorhinal cortex predicts performance in a reorientation task. *Current Biology*, 27:3658–3665 3654, 2017.
81. R.Q. Quiroga, Z. Nadasdy, and Y. Ben-Shaul. Unsupervised Spike Detection and Sorting with Wavelets and Superparamagnetic Clustering. *Neural Computation*, 16:1661–1687,, 2004. doi: 10.1162/089976604774201631.
82. N. Schmitzer-Torbert, J. Jackson, D. Henze, K. Harris, and A. Redish. Quantitative measures of cluster quality for use in extracellular recordings. *Neuroscience*, 131:1–11, 2005.
83. W.E. Skaggs, B.L. McNaughton, M.A. Wilson, and C.A. Barnes. Theta phase precession in hippocampal neuronal populations and the compression of temporal sequences. *Hippocampus*, 6:149–172,, 1996. doi: 10.1002/(sici)1098-1063(1996)6:2.
84. P. Berens. CircStat: a MATLAB toolbox for circular statistics. *J Stat Softw*, 31:1–21, 2009.
85. M. Franzius, H. Sprekeler, and L. Wiskott. Slowness and sparseness lead to place, head-direction, and spatial-view cells. *PLoS computational biology*, 3, 2007.

Methods

Animals. Japanese quails (Cotrunix japonica) of both sexes were used in this study. The quails were hatched and raised in our in-house breeding colony, housed in 1x1 m cages and maintained on a 12/12hr light/dark cycle. Food and water were provided ad libitum. All procedures were in accordance with the guidelines and approved by the Technion Institutional Animal Care and Use Committee. During recording sessions, no painful procedures were carried out.

Surgery. Adult Japanese quails (150 – 250 g, 4 – 12 months old) were prepared for repeated electrophysiological recordings with a single surgical procedure: the birds were anaesthetized with 3% isoflurane in a 4:5 mixture of nitrous oxide and Oxygen. Quails were then positioned in a stereotaxic frame (Kopf, small animals instrument Model 963) using Kopf rat ear bars. Head angle was controlled with a biting bar that was positioned $11\,\mathrm{mm}$ from and $45°$ below the inter-aural line (resembling the standard position in the pigeon and the quail atlases (40, 79). At this head position, in our stereotaxic setup, the cerebellum rostral tip was found at coordinate 0 (inter-aural line) $\pm 0.5\,\mathrm{mm}$ rostro-caudal. During surgery, animal temperature was maintained using a closed-circuit heating pad. Lidocaine (Lidocaine HCl 2% and Epinephrine) was injected locally at the incision site. The skull was exposed and cleaned. Four skull screws were inserted at the caudal part of the skull and one ground screw was inserted at the right frontal part of the skull. A $2\,\mathrm{mm}$ craniotomy was performed, in various positions ranging up to $4\,\mathrm{mm}$ rostral from the inter-aural line, and a small nick in the dura was made at the center of the craniotomy with a surgical needle. A custom-made Microdrive (as described in (80)) containing four tetrodes (made of $17.8\,\mu\mathrm{m}$ platinum-iridium wire, California Fine Wire) was carefully lowered until the tetrodes smoothly entered the brain tissue. Antibiotic ointment (Chloramfenicol 5%) was applied to the brain surface, followed by a thin silicon coat (Kwik-Sil). The drive was then connected to the ground screw with a wire and attached to the skull with adhesive cement (C&B-metabond) and light cured dental resin (Spident Inc. EsFlow). Loxicom ($5\,\mathrm{mg\,mL^{-1}}$) was injected intramuscularly and the quails were positioned in a heated chamber to recover overnight.

Electrophysiological recordings. Electrophysiological recordings were conducted in a 1 x 1 m open-field arena. The birds were released to roam spontaneously in the arena, mostly without any food; however, in some cases, food items were scattered in the arena to encourage movement. A tethered 16-channel headstage (Intan RHD2132) was attached to the drive and connected through a commutator (Saturn) to a data acquisition system (Neuralynx Digital SX). In some of the experiments the quails were untethered, in which case a 16-channel neural logger (Deuteron Technologies, MouseLog-16) was used for on-board acquisition and data storing. In both cases, animals were filmed with a CCTV camera with a frame-rate of $25\,\mathrm{Hz}$, and their position and head orientation was tracked by video-tracking two LEDs (green and red) mounted on both sides of the headstage or the neural-logger. Recording sessions were performed daily and lasted 10–45 minutes. Tetrodes were advanced by $50\,\mu\mathrm{m}$ per day. If no spikes were detected, electrodes were continuously lowered until spikes were observed. After reaching a depth of more than $100\,\mu\mathrm{m}$ in some of the experiments, electrodes were retracted to regions of previously observed spiking activity and more experiments were conducted. The thickness of the quail HPF layer varies from $800\,\mu\mathrm{m}$ on the lateral side to $2000\,\mu\mathrm{m}$ on the medial side (40). Therefore, recording depth was restricted to within $1200\,\mu\mathrm{m}$ below the brain surface, with more than 80%of the neurons collected in depths between 200 to $800\,\mu\mathrm{m}$ (Fig. 4b). Thus, the bulk of the recorded population of neurons was collected within the HPF. Yet, we cannot rule out the possibility that a small subset of the neurons from deep sites were recorded below the ventricle, or that neurons in the most lateral penetrations were from bordering areas adjacent to the HPF.
Electrical recording was sampled at 30 kHz using the Cheetah 6.0 software (Neuralynx), which records both 16-channel continuous raw data and spike detections. Raw signals were pre-amplified, bandpass filtered to 300–3000 Hz and thresholded (30–60 µV) to obtain on-line spiking activity (see supplementary Fig. S5 for examples of filtered traces). In untethered recordings, signals from the 16 channels were amplified ($\times 200$), filtered (300–7000 Hz) and sampled continuously at $29.3\,\mathrm{kHz}$ or $31.25\,\mathrm{kHz}$ per channel and stored. For synchronization between the neural-logger data recording and the Neuralyx video recording, a neural-logger control box sent TTL pulses to both the neural-logger and Neuralynx system at random intervals (10 ± 5 seconds). The timestamps were synchronized by utilizing polynomial curve fitting between the pulses recorded on both systems.

Data processing and spike sorting. During subsequent processing (off-line), the electrical recordings were filtered between 600–6000 Hz, and an adaptive voltage threshold (*Thr*) was used for spike detection, as describe by (81):

$$Thr = w \times median(\frac{|x|}{0.6745}) \quad \textbf{(1)}$$

Where x is the filtered recorded signal, and w is the noise threshold scaling parameter (between 2–5). Voltage threshold was averaged over $1\,\mathrm{min}$ recording windows. Electrical artifacts were detected and removed from all channels based on absolute voltage. Following artifact removal, a spike detection algorithm was used for each tetrode: whenever one channel crossed the threshold value, a $1\,\mathrm{ms}$ wide segment was saved from all channels on the tetrode, where the peak was centered over the 8^{th} sample (for a total of 32 samples). Coincidence detection algorithm was used to further identify and remove movement artifacts, where large-amplitude events occurring within all channels in each tetrode or between tetrodes were removed from analysis

(Supplementary Fig. S5b). Additionally, all detected spikes were compared to a pre-existing spike-shape database (template matching) by correlating different segments of the spike shape to each template from the database. A spike was included for further analysis if its Pearson-correlation coefficient with any of the spike templates was larger than 0.8. Manual spike sorting was performed offline using SpikeSort3D software (Neuralynx) and consisted of plotting the spikes in 3D parameter space, finding the features which give the best cluster separation and performing manual cluster cutting. Clustering quality was assessed based on two measures: isolation distance and Lratio (82). These parameters estimate how well-separated is the cluster of spikes from the other spikes and noise recorded on the same tetrode. A well-separated cluster has a large isolation distance and a small Lratio. A cluster was considered a single unit if it had an Lratio smaller than 0.2 and an isolation distance larger than 15. When the number of points outside the isolated cluster is smaller than half of the total points in the tetrode it is not possible to obtain the isolation distance value (NaN isolation distance; (83)). Clusters with NaN isolation distance were included in the analysis (see supplementary table S2). Additionally, clusters were categorized as multi- or single-units based on their inter-spike interval histogram: a cluster was categorized as single-unit if less than 5% of its spikes occurred less than $2\,\mathrm{ms}$ after the previous spike.

Histology. In a few of the quails, an electrical lesion was performed by injecting a positive current through one of the tetrodes (+5 for 20 sec). A week later, the quail was deeply anesthetized and perfused with phosphate buffer solution (PBS) followed by 4% paraformaldehyde. The brain was removed and stored in 4% paraformaldehyde for 2–3 days at 4, then transferred to PBS. Following fixation, the quail brains were dehydrated in 70%, 80%, 95% and 100% ethanol, cleared in Xylene and embedded in paraffin wax. The paraffin-embedded brains were coronal sectioned at 5 µm using a microtome (RM 2265 Leica). Sections collected at 40 intervals were mounted on superfrost glass slides and dried in an oven at 37 for 24 hours. After drying the sections, they were deparaffinized in xylene, rehydrated in a diluted ethanol series, and stained with 0.1% Cresyl violet solution (Nissl stain). The sections were then dehydrated, cleared and cover slipped with DPX mounting medium (Merck)

Data analysis. Single units were included for further analysis only if at least 300 spikes occurred during the session, and the recording session lasted more than 10 minutes. Spatial rate maps were computed by partitioning the arena into 3x3 cm bins. The number of spikes in each bin was divided by the time the bird spent in that bin. Bins which the quail visited for less than $200\,\mathrm{ms}$ were discarded and were colored white in the firing-rate map. Experiments in which the quail visited less than 50% of the arena were discarded from the spatial rate-map analysis. Spatial modulation was assessed based on two common measures: spatial information and spatial correlation (83). Spatial information index was calculated as:

$$I = \sum_x p_x \frac{\lambda_x}{\lambda} \log_2(\frac{\lambda_x}{\lambda}) \tag{2}$$

Where λ is the mean firing rate of the cell, λ_x is the mean firing rate in bin x (x includes only bins that the quail visited), p_x the probability of occupying bin x. Spatial correlation was the 2-dimensional correlation coefficient between the rate map of the first and second halves of the session – an index of stability. For statistical evaluation of the spatial modulation, a shuffling procedure was applied. The entire spike train was rigidly and circularly shifted by a random interval (intervals smaller than ± 20 sec were not used). This was repeated 1000 times and for each of the shuffles the spatial information index was calculated. The experimentally observed index was considered statistically significant with a P value larger than 0.01 if it surpassed 99% of the shuffle indices. For display purposes, the rate maps were smoothed using a 2D Gaussian kernel (3x3-cm bins, $\sigma = 3$ bins), but all the computations and indexes were calculated without smoothing.

Head-direction was computed as the perpendicular orientation from the line connecting the positions of the two LEDs (we used the red and green colors of the LEDs to unambiguously determine the correct direction). Head direction data were binned at 6o bins. The number of spikes in each bin was divided by the time the animal spent at that direction. The histogram was smoothed using a hamming window (n = 10 points) and displayed in polar plot view.

To assess the directionality of the tuning curve, the mean vector length of the circular distribution (Rayleigh score)(84) was calculated:

$$R = \frac{|\sum w \times e^{i\alpha}|}{\sum w} \tag{3}$$

Where w is the firing-rate per bin and α is the bin direction. The preferred (best) direction of the tuning curve was estimated by the direction of the Rayleigh vector:

$$preferreddirection = \arg \sum w \times e^{i\alpha} \tag{4}$$

The statistical significance of the directionality was assessed by applying a spike-shuffling procedure as described above. Shuffling was repeated 1000 times, and for each shuffle the Rayleigh score was calculated. A neuron was considered head-direction modulated if the Rayleigh score was larger than 99% of the shuffled scores. A shuffling procedure was used only for

tuning curves with a Rayleigh score higher than 0.10. The Rayleigh score (Rayleigh vector length) was called in this study 'HD score'.

To calculate spatial-view (SV) rate maps, in each frame the intersection point of the head direction with the arena wall was computed. The data was binned into 200 bins of 4 cm. The number of spikes in each bin was divided by the time spent in that bin. Data was color plotted along a rectangle representing the arena walls (Supplementary Fig. 3). The stability of the HD tuning curves, was assessed by dividing the time of the experiment into two halves (Fig. 3d); by dividing the arena into two regions: south half versus north half, east half versus west half, and center region versus border region (Fig. 3e-g); and by dividing the quail's speed to two speeds: below $10\,\mathrm{cm\,s^{-1}}$ and above $10\,\mathrm{cm\,s^{-1}}$ (Fig. 3h). Best HD was calculated separately for each part. This analysis was performed only in the sessions where the head direction coverage was larger than 50% in both regions. Head direction coverage was calculated by dividing the time spent at each region by 60 (the number of HD bins) and thus obtaining the expected time at each direction bin if the head directions are uniformly distributed. The percent coverage was then defined as the percentage of directional bins in which the quail spent more than 75% of the expected uniform time (see supplementary Fig. S1 for examples).

Simulations. Trajectories were simulated by first selecting a random initial location in the arena and an initial velocity drawn from a range between zero and an estimated maximal value ($70\,\mathrm{cm\,s^{-1}}$). Each single exploration period lasted 10 minutes and was divided to 30 Hz frames (total of 18,000 steps). For each frame (step), a new position (x,y) was simulated, depending on the previous position, current velocity and Gaussian noise, and weighted by the parameters m (momentum) and s (shift) as described below, utilizing a model of Brownian motion (as in (85))

$$pos(t+1) = pos(t) + m \times velocity(t) + (1-m) \times noise$$
$$noise = \mathcal{N}(\mu = 0, \sigma = s \times maxVelocity)$$

Where μ is the mean and σ is the standard deviation of the Gaussian distribution. In the event that the quail's next position ($pos(t+1)$) is out of the arena, velocity is recalculated by reducing half of its value and adding a uniformly distributed velocity value in the range: $-\frac{maxVel}{2}, \frac{maxVel}{2}$ this process continues until a new intra-arena position is found. The new velocity is then calculated as the difference between new and previous positions:

$$velocity(t+1) = pos(t+1) - pos(t) \quad \textbf{(5)}$$

Following the completion of the quail's trajectory simulation, a simulated HD or SV cell was used to determine the HD or SV rate map. The HD cell's preferred direction was drawn randomly for each trial from a uniformly distributed integers in the range of –180 to 180°. For each step, the angular difference between current HD and preferred HD was calculated and then utilized to determine the probability to trigger a spike:

$$p(spikes) = \frac{pdf(angleDiff)}{max(pdf)} \quad \textbf{(6)}$$

Where $angleDiff$ is the minimal angular distance between the current HD and the preferred HD and pdf is the probability distribution function (Gaussian) around zero; the standard deviation (SD) is defined as the cell's sensitivity and set to 45°to create broad-tuning cells similar to the real data. The final decision of whether there is a spike is determined by a random choice function weighted by p (for True) and $1-p$ (for False) probabilities. The spikes of an SV cell are simulated by the same process; however, in this case, the probability distribution was modified to fit a square arena in order that each point on the wall gets a probability value.

Supplementary Figures

Supplementary figure 1

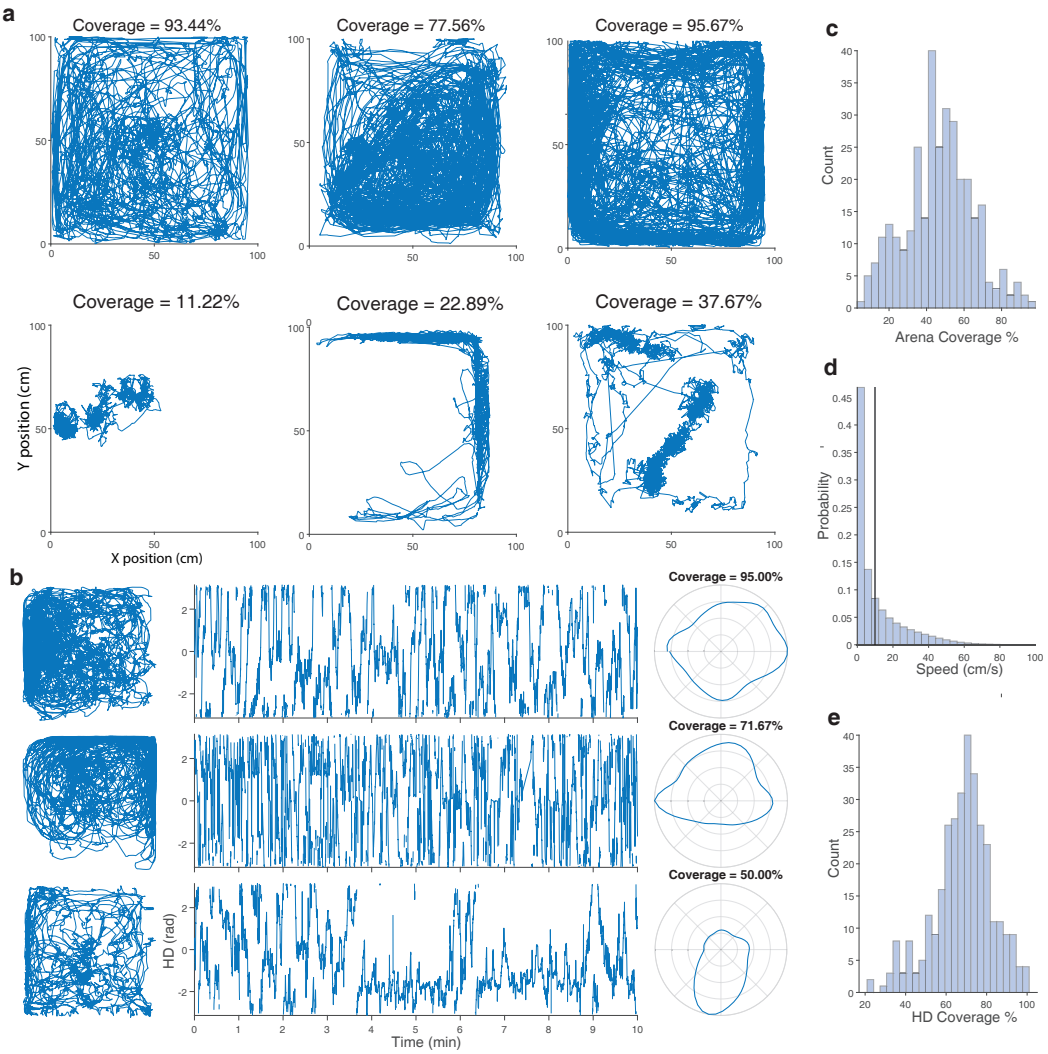

Fig. S1. Behavioral examples, spatial coverage of the arena, and head-direction coverage. **a**, Three examples of sessions with good spatial coverage (top) and three examples of sessions with bad spatial coverage (bottom). The % coverage is indicated above each example. **b**, Head-direction as a function of time from three sessions. Insets on the left show the corresponding position trajectories. Insets on the right show the corresponding polar plots of the time at each head direction. **c**, Spatial coverage of the arena for all behavioral sessions. Percent coverage is calculated as percentage of arena bins visited for more than $200\,\mathrm{ms}$. **d**, Probability distribution of the speeds, pooled from all behavioral sessions. The vertical line shows the value of $10\,\mathrm{cm\,s^{-1}}$ which was used to divide the data to slower versus faster speeds (Fig. 3h). **e**, The head-direction coverage for all behavioral sessions. Percent coverage is calculated as the percent of bins (each bin is 6° wide) in which the quail HD resided more than 75% of the session time divided by the number of bins (60 bins).

Supplementary figure 2

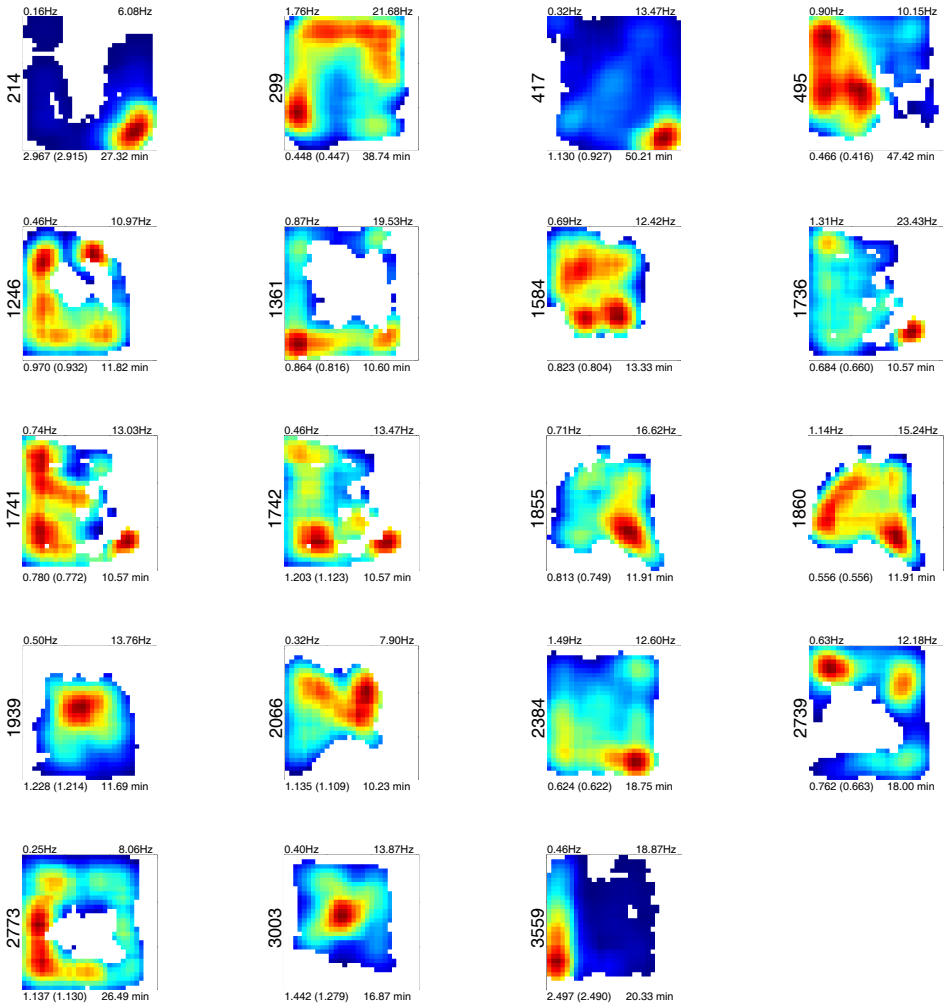

Fig. S2. Firing-rate maps of the 19 cells which showed significant spatial information. Each square represents the normalized heat map of one cell. Color coded from zero firing-rate (blue) to maximum firing-rate (red). White pixels designate bins that the quail did not visit during the session. Numbers above the plot designate the mean and max firing rates; numbers below the plot designate the spatial information index, in parentheses the information index at the 99th percentile of the shuffled distribution, and on the right is the time duration of the session. Numbers on the left of the panels designate the cell numbers.

Supplementary figure 3

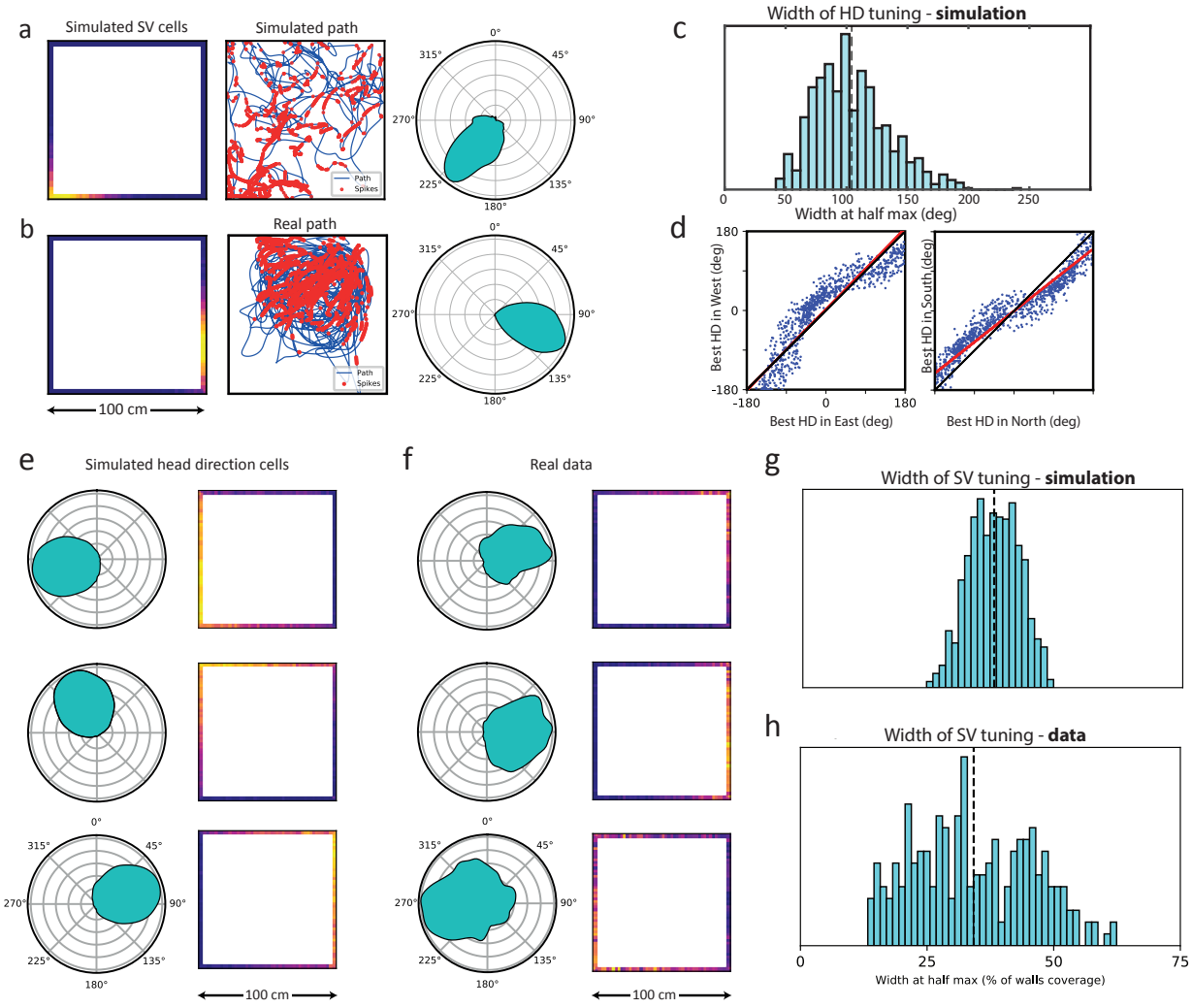

Fig. S3. Simulated relations between head-direction tuning and spatial-view (SV) cells, and comparison with data. **a**, Example of a simulated spike train of a hypothetical SV cell. The SV tuning of the hypothetical cell on the arena's walls is shown in the left panel (SV rate map). Hot colors designate high firing rates. The simulated spikes, in red, are plotted over a simulated trajectory (blue curve in the middle panel). The calculated HD tuning curve is shown in a polar plot on the right. **b**, same as panel a, but the spike train is simulated over a real trajectory of a quail in the arena. This results in clear and significant HD tuning curves. **c**, Widths at half maximum of emerging HD tuning curves from 1000 simulations. The dashed line shows the mean width (104.2 ± 30.3 deg) which was comparable to the mean width of the real HD tuning curves. **d**, Correlations of simulated (n=1000) best HDs between east and west (left) and north-south (right) parts of the arena. The black line is the identity-line and the red line is the linear regression. Data points show an oscillatory pattern around the midline, which was not observed in the real data – arguing that the neurons we recorded are not SV cells. **e**, Simulated SV rate maps from three hypothetical HD cells whose tuning curves are shown in the left column. The emerging firing-rate maps on the arena walls are shown in the right column. **f**, Data from three of the recorded HD cells. The left column shows the HD tuning curves and the right column the corresponding SV rate maps. **g**, A histogram of SV rate-maps tuning widths at half max from 1000 simulations of HD cells. The dashed line shows the mean (37.8 ± 4.9 % of wall coverage). **h**, The SV rate maps tuning widths of the 260 HD cells recorded in this study. The dashed line shows the mean (34.2 ± 11.7% of wall coverage).

Supplementary figure 4

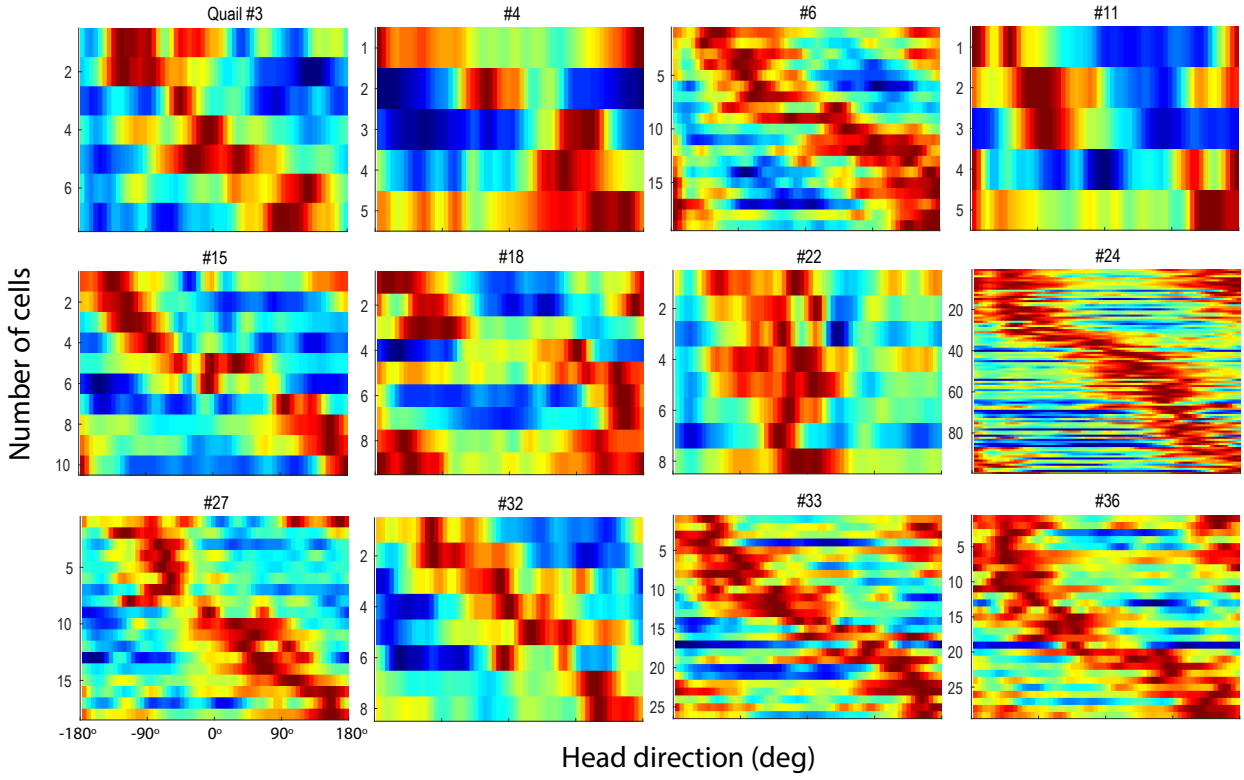

Fig. S4. Head direction tuning curves from individual quails. Each plot shows the tuning curves of all significant head-direction cells recorded in one quail; the quail ID number is shown above the plot. Each row designates a single cell and is normalized from zero (blue) to its maximal firing-rate (red). Curves are ordered according to the best direction. Shown are data from all the quails in which ≥ 5 significant HD cells were recorded (12 out of 21 quails).

Supplementary figure 5

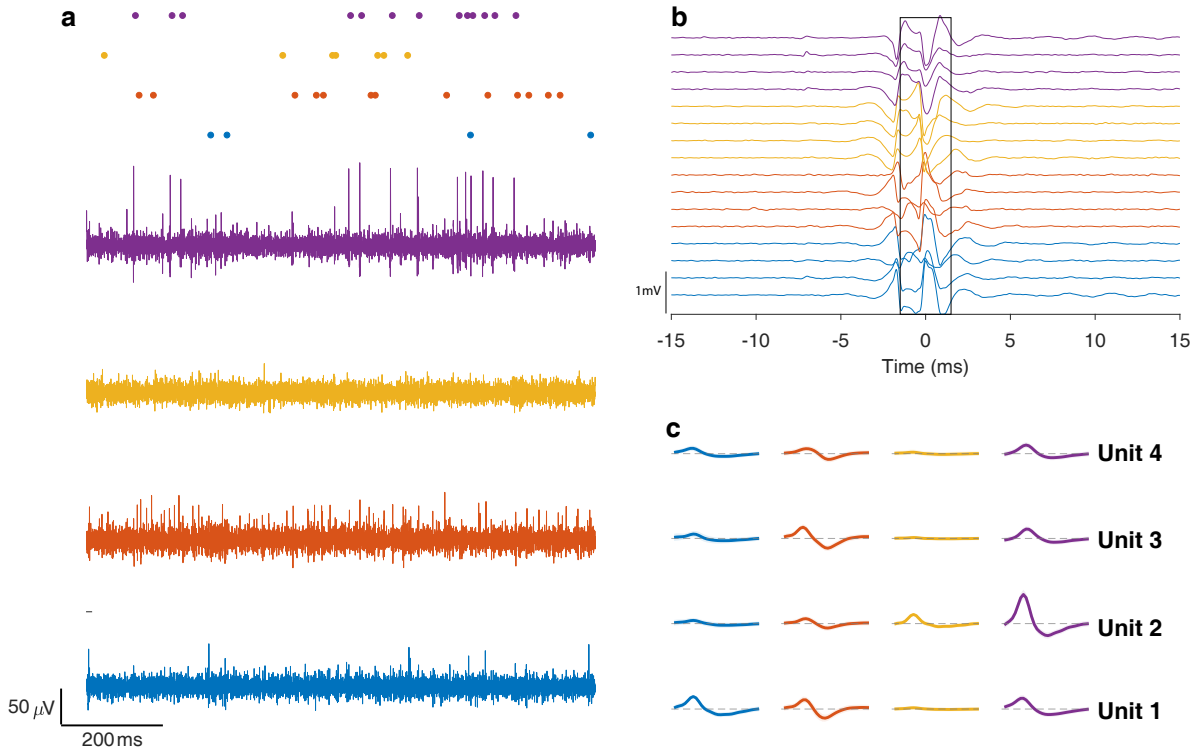

Fig. S5. Examples of electrophysiological recording traces. **a**, Bandpass filtered recording from single electrodes of each tetrode. Top row shows detected spikes, color-coded for each electrode. **b**, Bandpass filtered traces of all 16 channels, showing a movement artifact – usually associated with ground pecking by the bird. Colors designate different tetrodes. Black box marks time window discarded from the recording as part of the artifact-cleaning process. **c**, Spike shapes of the single units shown in panel a. Colors indicate the 4 channels of the tetrode.

Supplementary Tables

Table S1. Summary of recorded cells per quails. Locations of penetrations relative to the cerebellum were measured post mortem. In four of the quails (marked by *) electrode traces were reconstructed in Nissl stained slices.

		Location of penetration		Modulation Type			
	Animal#	**From Cerebellum (mm)**	**From midline (mm)**	**Head-direction cells**	**Place cells**	**None**	**Total**
1	1	0.15	-0.4	0	0	32	32
2	2	3	-0.5	0	0	6	6
3	3	5	-0.6	7	0	36	43
4	4	3	-0.5	5	1	16	22
5	5*	2	-0.4	1	0	4	5
6	6	3	-0.6	19	1	35	54
7	7	2	-0.3	3	1	21	25
8	9			2	0	25	27
9	11	1	-0.3	5	1	30	36
10	15	2.5	1.5	10	0	105	115
11	17	1	-0.5	4	0	8	12
12	18	2	-0.5	9	0	8	17
13	20	3.1	-1	2	0	28	30
14	22*	3	-1	8	1	155	164
15	24*	4.5	-0.5	99	9	409	514
16	27			18	1	284	305
17	30			2	0	2	4
18	31	3.8	-1.6	3	0	3	6
19	32			8	0	85	94
20	33*	2.6	-1.5	26	2	152	179
21	36	2.4	-1.6	29	2	412	442
Total				260	19	1851	2127

Table S2. Percent head direction positive cells in different spike isolation criteria. The percentage of HD cells has been calculated using eight different combinations of criteria for single unit isolation: Upper limit of Lratio, Lower limit of Isolation Distance and whether to include clusters with NaN isolation distance values (when the number of points outside the isolated cluster is smaller than half of the total points in the tetrode an isolation distance value cannot be computed).

Lratio	Isolation distance	NaN values	Cells total	HD Cells	HD Cells percentage [%]
0.2	15	included	2144	270	12.6
0.2	30	included	1354	168	12.4
0.1	15	included	1674	201	12
0.1	30	included	1287	157	12.2
0.2	15	not included	1761	217	12.3
0.2	30	not included	971	115	11.8
0.1	15	not included	1305	151	11.6
0.1	30	not included	918	107	11.7